Surface diffusion of Ge on Si(111): Experiment and simulation

C. E. Allen, R. Ditchfield, and E. G. Seebauer*
Department of Chemical Engineering, University of Illinois, Urbana, Illinois 61801
(Received 15 August 1996)

Surface diffusion of Ge on Si(111) at high temperatures has been examined experimentally by second-harmonic microscopy and computationally by molecular-dynamics simulations with a Stillinger-Weber potential. Experimentally, the activation energy and preexponential factor for mass-transfer diffusion equalled 2.48 ± 0.09 eV and $6 \times 10^{2 \pm 0.5}$ cm^2/s, respectively. Simulational results yielded essentially the same numbers, confirming the utility of the Stillinger-Weber potential for diffusional studies. A previously developed semi-empirical correlation also did fairly well. The simulations also provided estimates for the corresponding parameters for intrinsic diffusion and for the enthalpy and entropy of Ge adatom-vacancy pair formation on Si. The simulations further yielded evidence for minor contributions of atom exchange to intrinsic diffusion, as well as the complex high-temperature islanding phenomena on picosecond time scales.
[S0163-1829(97)04419-6]

I. INTRODUCTION

Measurements of adsorbate diffusion can offer key insights into the thermodynamics and kinetics of surface processes. In thermodynamics, surface diffusion contributes to the adsorbate partition function and can influence the coverage dependence of the heat of adsorption.[1] In kinetics, surface diffusion can induce unique effects in the rates of recombinative desorption.[2]

While experimental reports of surface diffusion number over 500,[3] a surprisingly small fraction treats this phenomenon at ''high'' temperature, defined here to be 50–60 % or more of the substrate melting point. Yet this regime encompasses the temperatures of interest in many practical applications where surface diffusion plays a key role (e.g., sintering, crystal growth, and reflow processes).[4–6] Phenomenology in such applications tends to be governed by mass-transfer diffusion as opposed to intrinsic diffusion, which is more familiar. While the latter describes motion of individual particles, the former accounts explicitly for the number of mobile particles. Formally, the mass-transfer diffusivity D_M and the intrinsic diffusivity D_I obey the relation[7]

$$D_M = \frac{N}{N_S} D_I, \tag{1}$$

where N represents the actual areal density of mobile particles while N_S represents a maximal density. In self-diffusion, N_S typically equals the substrate atom density while N may be governed by processes like adatom-vacancy pair formation. Since adatoms typically display far greater mobility than substrate atoms, in most case $N \ll N_S$ implying that $D_M \ll D_I$. Of course, N may display a strong temperature dependence governed by the free energy of vacancy formation ΔG_f according to[8]

$$\frac{N}{N_S} = e^{-\Delta G_f / k_B T}. \tag{2}$$

Equations (1) and (2), together with the assumption of thermally activated intrinsic diffusion and the decomposition of ΔG_f into its component enthalpy ΔH_f and entropy ΔS_f lead to

$$E_M = E_I + \Delta H_f \tag{3}$$

and

$$D_{0,M} = D_{0,I} \exp(\Delta S_f / k_B), \tag{4}$$

where E and D_0 denote, respectively, the activation energy and preexponential factor. Qualitative arguments suggest that both ΔH_f and ΔS_f are large and positive for adatom creation from terrace vacancies,[3,9] and molecular-dynamics simulations for Lennard-Jones[10] and Stillinger-Weber[11] potentials have confirmed this notion for self-diffusion.

We have focused considerable experimental effort on quantifying and correlating these effects for semiconductors. Through use of second-harmonic microscopy (SHM), we have examined heterodiffusion of group-III and -V adsorbates on group-IV substrates.[9,12–14] The large values for E and D_0 observed for these systems mimic for heterodiffusion the effects just described for self-diffusion. The close correspondence arises from the known ability of the adsorbates to substitute into the top layer of the substrate.[15–17] While the general physical picture for self-diffusion describes qualitatively the results from heterodiffusion, more quantitative predictions remain elusive mainly because of adsorbate ionization effects that can arise when the adsorbate and substrate differ significantly in electronegativity.[12] Complete or partial adsorbate ionization contributes significantly to both ΔH_f and ΔS_f in ways that remain difficult to quantify, making other contributions to these quantities difficult to measure directly.

The present work seeks to avoid this problem by examining an adsorbate-substrate system with good matches in both electronegativity and chemical phenomenology: Ge on Si(111). Experimental measurements with SHM are compared with diffusion parameters obtained by molecular-dynamics (MD) simulations using the Stillinger-Weber po-

tential. Good correspondence appears, giving more credence to some of the curious atomic behavior observed in the simulations.

II. METHODS

A. Experiment

The general experimental setup has been described in detail previously,[9,12,18–20] making only a brief description necessary here. The apparatus consisted of an ultrahigh vacuum (UHV) chamber together with an optical illumination and imaging system for second-harmonic generation. The UHV chamber was pumped turbomolecularly, producing a base pressure of 8×10^{-11} torr, and was equipped for low-energy electron diffraction (LEED), Auger electron spectroscopy (AES), mass spectroscopy, and ion bombardment.

A Quantel (Continuum) 660B Nd:YAG (yttrium aluminum garnet) laser operating at 10 Hz provided the probe beam at 1064 nm with a pulse width of 5 ns. The beam was attenuated and conditioned by various optics both to remove spurious wavelengths and to rotate the light to the desired linear polarization. The beam reflected from the sample at near-normal incidence with a fluence of 250 mJ/cm2 per pulse. An achromatic lens ($f/5.08$) focused the second-harmonic (SH) image at 532 nm onto a gated, doubly intensified photodiode array (Princeton Instruments D/SIDA) with a magnification of 17 times. A cylindrical lens then collapsed the SH image in the direction parallel to the step, providing additional signal enhancement. The spatial resolution of this setup (after signal processing described below) was approximately 3 μm after 3 min of imaging.

Experiments employed substrates measuring 1.3 cm $\times$0.8 cm$\times$0.33 mm cut from boron-doped Si(111) (Monsanto) having a resistivity of 0.01 Ω cm. A Chromel-Alumel thermocouple monitored the temperature. Once in UHV, the surface was bombarded with Ar^+ and annealed at 1100 K for 10 min. AES showed no detectable contaminants after this procedure.

A one-dimensional step concentration profile was formed using a retractable mask constructed of cleaved GaAs.[18] Germanium originated from a specially designed evaporative source constructed of boron nitride, whose temperature was monitored using a W5%Re-W26%Re thermocouple. Dosing was performed at 310 K, where control experiments showed diffusion to be negligible. AES showed no detectable contaminants following the dosing process. The surface was then annealed for 1 min at 900 K providing SH signal enhancement, as documented in previous studies of Ge growth on Si.[21] All imaging was performed at 430 K, which could be obtained quickly upon sample cooling. Control experiments demonstrated that neither surface damage nor thermal or laser-induced diffusion resulted from imaging. The diffusion temperature was computer controlled to ±1 K of the setpoint temperature.

Raw second-harmonic images were processed using methods described previously[13] to remove detector shot noise and broadening from the system's optical response function. The resulting profile was converted to the coverage domain using a calibration curve (shown in Sec. III) obtained with AES. As in previous work,[9,12,13,18] diffusion profiles were analyzed in the continuum approximation using the Boltzmann-Matano method, which yields the dependence of D on coverage θ without parametrization. The required mass-balance condition about the zero point of the initial step[9] held within 2–3% for all cases, thereby demonstrating no adsorbate loss by desorption or sinking into the bulk.

B. Simulation

MD simulations were performed using the Stillinger-Weber potential.[22] Appropriate parameters for this potential have appeared in the literature for the Si-Si,[22] Ge-Ge,[23] and Si-Ge (Ref. 24) interactions. The computer code we employed has been described previously[11] but was substantially rewritten for improved speed and flexibility. The simulations employed a constant number-volume-temperature (*NVT*) ensemble containing $N_S=112$ atoms per layer in the (111) orientation. Five mobile layers rested upon three fixed layers. Each time step in the integration corresponded to 3.8317 fs. Simulations lasted about 10^5 time steps, including a relaxation period of 5×10^3 steps to reach initial equilibrium. In all simulations, the adatom coverage $\theta=N/N_S$ was monitored regularly. Adatoms were defined as those particles whose center of mass lay above the midpoint between the planes bisecting the substrate layer and the overlying adsorbate layer.

Simulations of intrinsic diffusion employed a substrate composed entirely of Si with four Ge adatoms placed on top at random. Mobility took two forms: normal site-to-site hopping and exchange. Exchange mimicked that observed on metals;[25] a Ge adatom dove into the top layer of Si, displacing a Si atom into a different adatom position.

Intrinsic diffusivities were computed using a relation between D and the hop rate:[26]

$$D=\frac{M\lambda^2}{4t}, \tag{5}$$

where M denotes the number of hops a particle makes in time t. The hop length λ corresponds to the distance between surface sites for a simple hop. For an exchange event, this distance must be multiplied by a geometrical factor of $(\frac{1}{3})^{1/2}$ since a Ge atom exchanging into the surface does not move the entire site-to-site distance. This situation contrasts with self-diffusion, where no correction is needed because the initial and final states describing hops and exchanges look identical.[27] Isolated adatoms tended to disappear during simulation by either dimerization or exchange. Therefore, t for a disappearing particle corresponded only to its lifetime in isolated form. Similarly, the geometrical factor for exchange was applied only to the time period preceding the exchange event, with M in Eq. (5) equalling unity for the event. Final computation of D involved averaging over the particles and time periods. Simulations proceeded at temperatures sufficiently low to enable unambiguous monitoring of individual jumps. For this reason, the continuum expression[28]

$$D=\frac{\langle x^2\rangle}{4t} \tag{6}$$

with $\langle x^2\rangle$ being the mean square displacement could not be used in these simulations due to the small number of hops.

Such hops are necessarily self-correlated, causing Eq. (6) to overestimate D, but Eq. (5) yields the correct result.[2,29]

Calculations for mass transfer diffusion extended to higher temperatures and involved longer diffusion distances. Also, the entire substrate became sufficiently mobile to make discernment of discrete adsorption sites difficult. Thus, Eq. (6) was employed for computations of D_M. These simulations employed a pure Si substrate, except for the top layer, which included 50% Ge atoms distributed at random. No adatoms existed initially; these appeared during the equilibration period by adatom-vacancy pair formation.

Various practical considerations imposed limits on the temperature range employable in MD. For intrinsic diffusion, poor statistics for small numbers of jumps determined the low end, while rapid adatom disappearance by dimerization or exchange fixed the high end. For mass-transfer diffusion, fluctuations in the small adatom density set the low end, while surface melting fixed the high end.

III. RESULTS

A. Experiment

A calibration curve relating SH signal to coverage θ was constructed using AES measurements. The relation

$$\frac{\theta_{\mathrm{Ge}}[1-f(\lambda_{\mathrm{Ge}}(E_{\mathrm{Ge}}))]}{1-\theta_{\mathrm{Ge}}[1-f(\lambda_{\mathrm{Ge}}(E_{\mathrm{Si}}))]}=\frac{1+r_{\mathrm{Ge}}(E_{\mathrm{Ge}})}{1+r_{\mathrm{Si}}(E_{\mathrm{Ge}})}\frac{I_{\mathrm{Ge}}}{I_{\mathrm{Si}}}\frac{I^{\infty}_{\mathrm{Si}}}{I^{\infty}_{\mathrm{Ge}}} \quad (7)$$

was employed to analyze the AES data,[30] with coverage θ defined to be unity at the substrate atom density of 7.8×10^{14} atoms/cm^2. From experiments on pure elemental surfaces, the pure species peak height ratio $I^{\infty}_{\mathrm{Si}}/I^{\infty}_{\mathrm{Ge}}$ was measured as 2.2 using the peaks $E_{\mathrm{Si}}=92$ eV and $E_{\mathrm{Ge}}=1147$ eV. At 1147 eV and normal incidence, the backscattering factors $(1+r)$ were taken to be 1.5 for Ge and 1.3 for Si.[31] The inelastic mean free paths λ for electrons in Ge at 92 and 1147 eV were estimated to be 6 and 24 Å, respectively, with a monolayer thickness a_{Ge} of 3 Å.[32] The value of $f(E)$ was computed for our 120° analyzer as

$$f(E)=\frac{8}{3}\int_0^{60^\circ}\cos\phi\,\exp\left(\frac{-a_{\mathrm{Ge}}}{\lambda_{\mathrm{Ge}}(E)\cos\phi}\right)\sin\phi\,d\phi, \quad (8)$$

yielding $f(92\ \mathrm{eV})=0.388$ and $f(1147\ \mathrm{eV})=0.881$. The resulting calibration curve appears in Fig. 1. For $\theta<0.7$, the SH intensity $I(\theta)$ increased linearly with coverage from the clean-surface value I_0 according to

$$I(\theta)=I_0(1+5.12\theta) \quad (9)$$

Above $\theta=0.7$, $I(\theta)$ saturated at $4.58\,I_0$.

Figure 2 shows typical raw data collected for a single diffusion experiment. Images of both the initial step and diffused profile appear for diffusion at 1025 K for 90 min. Profiles similar to Fig. 2 were collected over the temperature range $960\leqslant T\leqslant1100$ K, limited at the low end by slow diffusion and at the high end by silicon melting.

Image processing and the Boltzmann-Matano analysis led to the actual diffusivities. At all temperatures examined, plots of D vs θ revealed no meaningful coverage dependence in D. The diffusivities for each coverage were then averaged to remove small random variations and were fit with a standard Arrhenius expression to yield the activation energy E_{diff} and prefactor D_0. Figure 3 shows sample data. Figure 4 shows the lack of coverage dependence explicitly; E_{diff} and D_0 remained constant at 2.48 ± 0.09 eV and $6\times10^{2\pm0.5}$ cm^2/s, respectively.

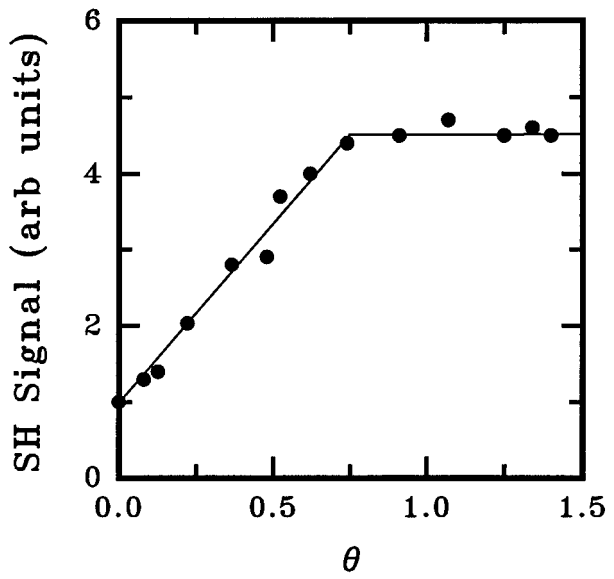

FIG. 1. Second-harmonic signal vs Ge coverage on Si(111).

B. Simulation

Since surface diffusion results for mass transfer have long been discussed in terms of the substrate melting temperature T_m,[3,7,33,34] the bulk melting temperature for Si was sought in simulation by visual observation of computer-generated lattice pictures. An abrupt transition appeared at 2500 K involving substantial disordering and intermixing of all five mobile layers. Initial melting of only the surface layer has been observed for Lennard-Jones structures[10,33] but did not

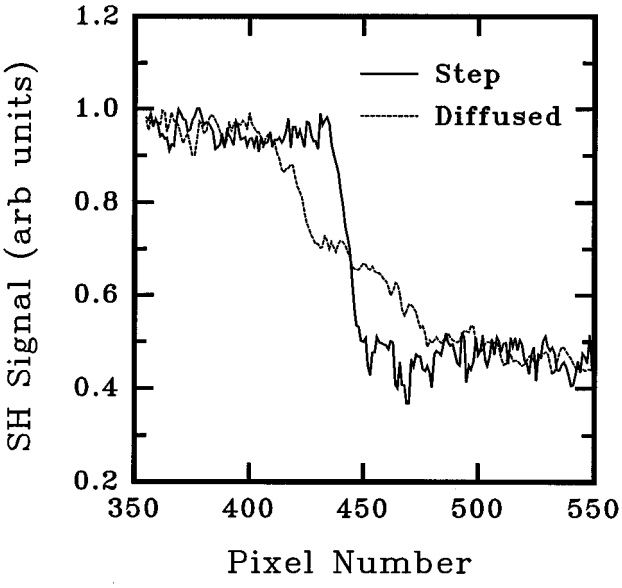

FIG. 2. Raw second-harmonic images of profiles measured initially and after 90 min of diffusion at 1025 K.

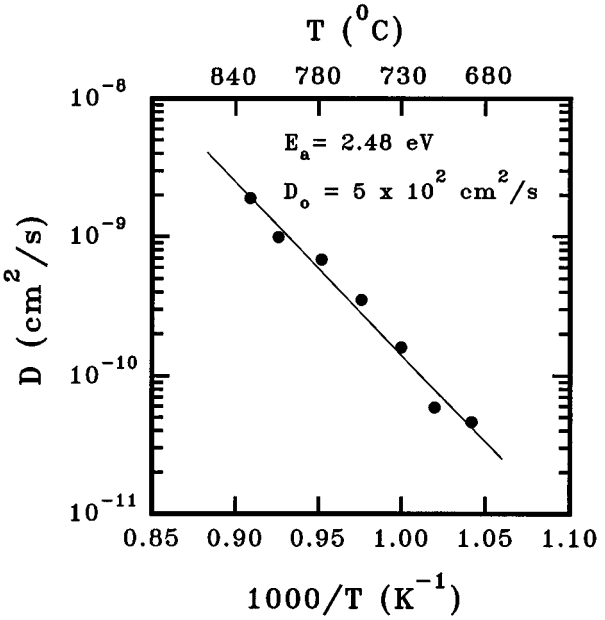

FIG. 3. Arrhenius plot of diffusion measured by SHM.

occur here. The observed melting temperature lies significantly above the experimental value of 1683 K for reasons presented in Sec. IV.

As mentioned earlier, intrinsic diffusion took place both by normal site-to-site hopping and by exchange. An example

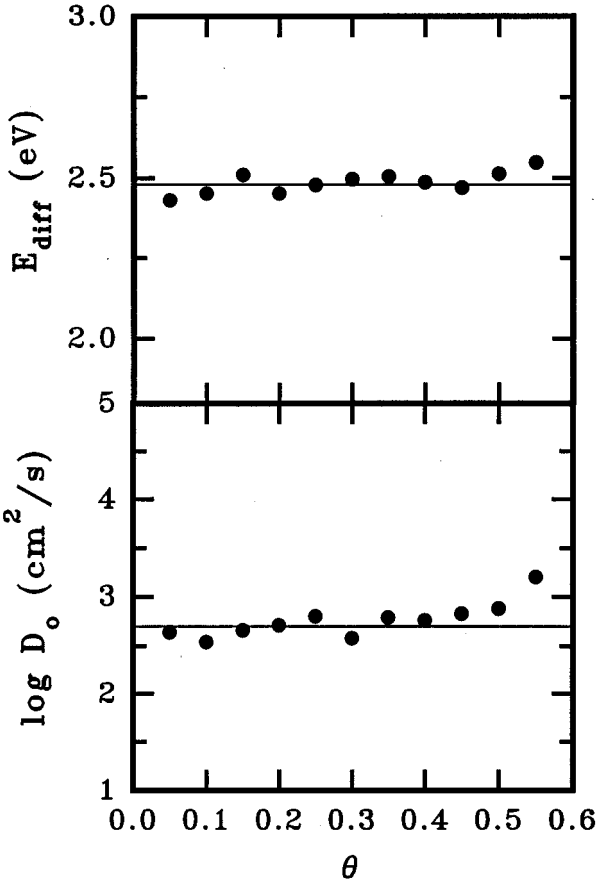

FIG. 4. Coverage dependence of $E_{\rm diff}$ and D_0; these quantities remained essentially constant.

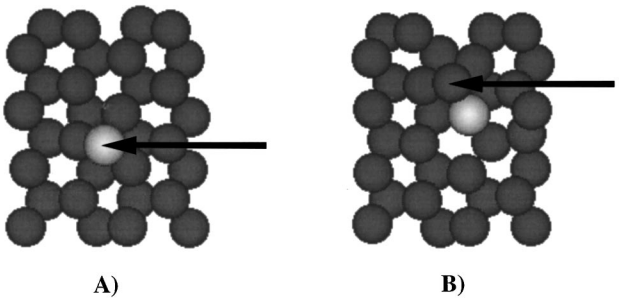

FIG. 5. Computer-generated pictures of exchange diffusion observed in molecular dynamics. Dark spheres represent Si, the light one is Ge. Arrows demark adatoms; the rest sit in the first substrate layer or below. (B) comes 4 ps after (A), with $T=1650$ K.

of the latter process appears in Fig. 5. Site-to-site hopping proved to be the dominant mode at all temperatures employed, however. Figure 6 shows an Arrhenius plot for both processes. Extrapolation of the lines shows that the rates become equal near the melting temperature because of the higher activation energy for exchange.

Figure 6 also shows results for mass-transfer diffusion. While the absolute value of D_M lies below that for D_I by either mechanism, the higher activation energy for D_M causes the mass-transfer line to cross the other two near T_m. Remarkably, all lines cross at the same temperature.

Pictures of the mass-transfer process revealed a phenomenon far more complex than the straight Arrhenius plot of Fig. 6 might suggest. Some simple adatom-vacancy pair formation and annihilation did take place. However, on average most adatoms appeared as the result of cooperative effects on a longer length scale. Figure 7 shows the time evolution of a typical example in top and side views. In general, the open lattice structure of Si(111) permitted extensive relaxation in

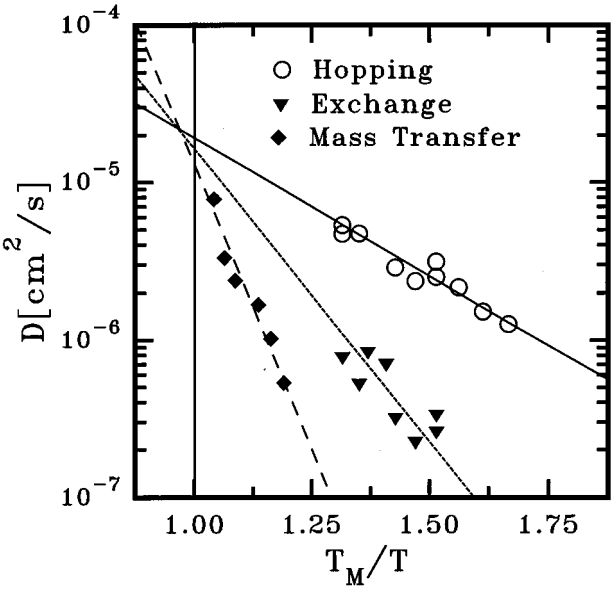

FIG. 6. Arrhenius plots of simulated diffusivities for intrinsic diffusion by site hopping and exchange, and for mass-transfer diffusion. Lines represent least-squares fits. Abscissa is scaled by the simulated melting temperature $T_m=2500$ K. All plots converge near T_m.

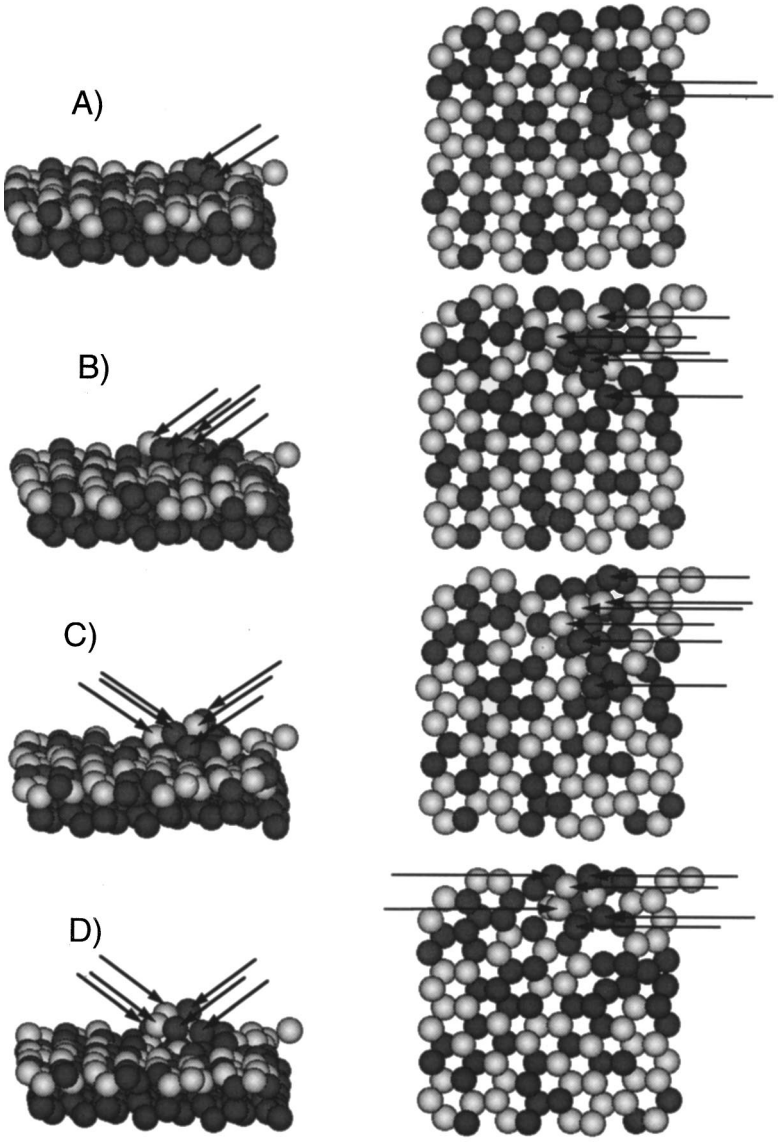

FIG. 7. Sequence of computer-generated pictures of mass transfer diffusion at 2200 K. Dark atoms represent Si, light ones Ge. Arrows demark adatoms. Simulation times are (A) 0, (B) 7.5 ps, (C) 27 ps, and (D) 31 ps. Top and side views appear for each time. Two nearby adatom-vacancy pairs catalyze formation of an island and surrounding diffuse ''moat.'' An individual atom breaks off toward the bottom (B) and (C), and disappears (D). Island shape and height generally remained ill defined.

the vicinity of a single vacancy. Two vacancies in close proximity induced even stronger effects. This relaxation appeared to catalyze the rapid formation of more adatom-vacancy pairs nearby. The adatoms then agglomerated together into islands of six to ten particles, while the vacancies remained nearby as a diffuse, ill-defined surrounding moat in the first substrate layer. Virtually no vacancies or lattice distortion propagated down into underlying layers.

Mass-transfer diffusion occurred principally when individual adatoms or small clusters detached from an island and moved short distances before reincorporation into the top layer. Figure 8 shows examples. The islands themselves usually remained fairly stable in size throughout the simulation time of roughly 0.5 ns and moved slowly by the detachment and reattachment of adatoms or small clusters at the edges. Monomers, dimers, and trimers all had roughly comparable mobilities throughout the temperature range. Although all cluster types involved both Ge and Si atoms, the diffusivities computed in Fig. 6 involve Ge only.

Figure 8 also shows an island disappearing abruptly back into the top layer. This disappearance occurred more often at low temperatures where average adatom concentrations remained low. The island simply sank in concerted fashion back into its diffuse moat of vacancies, generally leaving one or two isolated adatom-vacancy pairs behind. The particular case of Fig. 8 represents a direct continuation of the events in Fig. 7. The time scale is quite short; a period of 50 ps encompasses island formation, motion, and disappearance.

Figure 9 shows average adatom coverage in Arrhenius form. A break appears in the plot near $\theta = 0.08$. Visual inspection of simulational results showed that this effect arose from the method for counting adatoms. At sufficiently high temperatures, the moats around the islands grew sufficiently large to permit significant atomic mobility within their diffuse confines. Atoms within these moats became *de facto* adatoms migrating on top of the second substrate layer. The counting scheme for adatoms did not account for such effects. However, a rational generalization of adatom definition to include mobile atoms within the moats proved difficult to construct because the boundaries were so diffuse and changeable. Thus, while Fig. 9 shows adatom coverage according to the definition given earlier, we consider only the four lowest points to reflect true adatom (and therefore mobile, species) coverages.

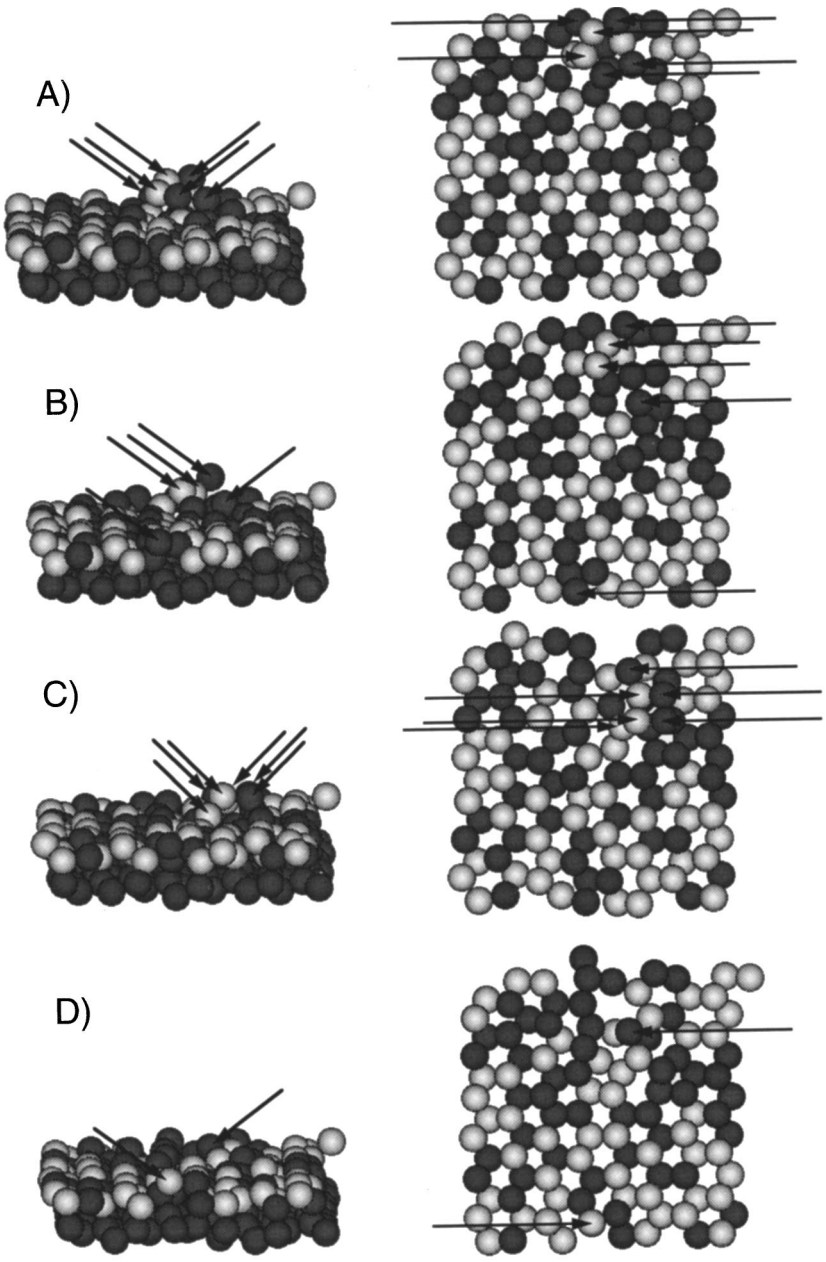

FIG. 8. Continuation of the sequence in Fig. 7, with times (A) 31 ps, (B) 34.5 ps, (C) 42 ps, and (D) 50 ps. The island changes shape constantly and then suddenly sinks back into the substrate. Since periodic boundary conditions apply, adatoms near the bottoms of the figure are actually near or part of the island.

IV. DISCUSSION

A. Experiment

The measurement temperatures employed here, when scaled by the experimental melting temperature of Si, corresponded to a range for T/T_m between 0.57 and 0.65. Kinetic parameters for mass-transfer diffusion on Si in this range typically fall between 1.8 and 3.6 eV for E_{diff} and between 10^1 and 10^7 cm^2/s for D_0.[3] The present measurements of 2.48 eV and 6×10^2 cm^2/s fall well within this range, and well outside the range for intrinsic diffusion, whose respective parameters on Si typically average near 0.9 eV and 10^{-3} cm^2/s.[3] This evidence strongly suggests that the present measurements concern mass-transfer diffusion.

For comparison with related systems, E_{diff} and D_0 have been reported at 3.6 eV and 9×10^3 cm^2/s for Si/Si(111)[35] through use of LEED techniques. Reflection high-energy electron diffraction has yielded $E_{\text{diff}}=3.8$ eV for Ge/Ge(111),[36] although the reliability of this technique for surface diffusion measurements has proven spotty. No prior measurement exists to our knowledge for the corresponding prefactor; nor have results been reported for Si on Ge.

B. Simulation

Intrinsic diffusion occurred in simulation both by site-to-site hopping and by exchange. This latter mechanism, though forming a rather minor contribution in the present work, represents a new result. Exchange has been verified experimentally to operate on metal surfaces,[25] but not for semiconductors. Instead, only site hopping and rather complex concerted exchanges *within* the top substrate layer have been observed.[37,38] Standard exchange on semiconductors has been reported for Si self-diffusion on Si(100) using MD simulations and a Stillinger-Weber potential, but kinetics were not investigated.[39]

Activation energies and preexponential factors determined here for site hopping and exchange appear in Table I.

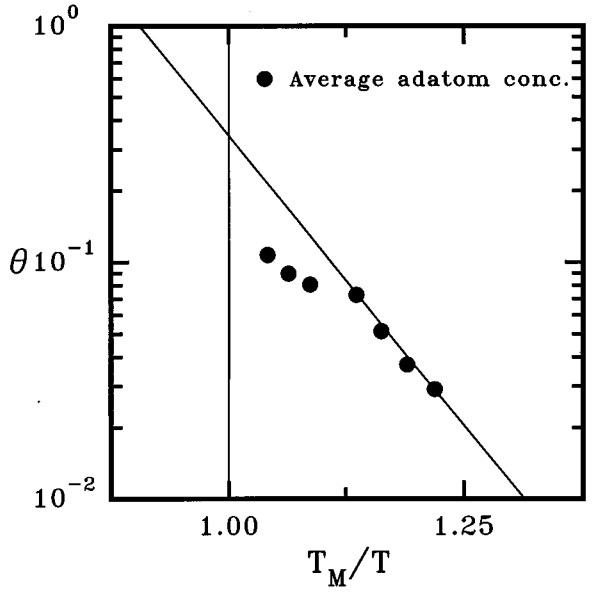

FIG. 9. Arrhenius plot of simulated Ge adatom coverage. As discussed in the text, the three high-temperature points underestimate the true mobile atom coverage.

Exchange exhibits an activation energy larger by a factor of 2, although the prefactor compensates for this effect, being larger by a factor of 60. While D_0 for site hopping falls at 10^{-3} cm^2/s, the value one can calculate from simple arguments involving hop length and attempt frequency,[4] exchange evidently involves a positive entropy change of $\Delta S/k_B$ near ln(60), or roughly 4. We speculate that this change may result from some softening of the local lattice in the transition state.

The substantially higher activation energy for exchange than for site hopping may explain why experimental observations of exchange do not exist for semiconductors. While the two phenomena have roughly comparable rates at simulational temperatures T/T_m near 0.7, experimental techniques capable of identifying exchange on semiconductors (like scanning tunneling microscopy) have generally employed much lower temperatures, usually below $T/T_m \sim 0.35$.[3] At these temperatures, exchange should occur several orders of magnitude more slowly than site hopping.

Other reports of simulated intrinsic diffusion parameters for Ge/Si(111) do not exist to our knowledge. However, two such reports exist for Ge/Si(100). Surface anisotropy induced by the dimer rows complicates the diffusional dynamics on this surface. However, MD simulations with Tersoff's potential yield E_I and D_0 of 0.73 eV and 4.3×10^{-4} cm^2/s for macroscopic intrinsic diffusion,[40] where adatoms jump along and across the rows as they please. These results fall broadly in line with ours. Diffusion along the rows, which exhibits a potential corrugation more like the (111) than motion across the rows, obeys a similar activation energy of 0.64 eV.[41]

Mass-transfer diffusion proceeded in our simulations by a complex melange of the motion of monomeric adatoms, small clusters, and islands. Curiously, however, the quantitative aspects of the data obeyed the relations embodied in Eqs. (1), (3), and (4) quite well even though the data for intrinsic diffusivity involved monomeric adatoms only. Table I shows the correspondence in numerical form. We rationalize these results by noting that monomers, dimers, and trimers all moved at comparable rates, and that islands moved mainly by detachment and reattachment of these entities. Thus, monomeric kinetics fortuitously described all motion.

C. Comparison of experiment and simulation

The simulated melting temperature $T_{m,s}$ lay nearly 50% higher than the experimental value $T_{m,e}$. This discrepancy has also appeared in the literature, with some groups reporting high $T_{m,s}$ (Refs. 22 and 42) and others reporting close correspondence to experiment.[41,42] Overestimates of $T_{m,s}$ appear to arise from insufficient ensemble size.[42] Workers achieving good correspondence with experiment have used roughly comparable numbers of atoms per layer (e.g., 64 in Ref. 43 and 144 in Ref. 44), but also employed more than 20 mobile layers compared with our five. Visual inspection of a 20-layer simulation shows that near the melting point, atomic motion may be significantly enhanced even five or six layers down compared with the deep bulk. We believe that our small ensemble size, limited by workstation capabilities, induced artificial stiffening of the mobile lattice that raised $T_{m,s}$.

We also believe this effect did not arise from superheating, which results from a lack of defects at which the simulational melting process can nucleate.[22] The present simulations displayed plenty of vacancies and other defects at the free surface as low as 1800 K, far below the observed $T_{m,s}$ of 2500 K.

TABLE I. Arrhenius parameters for diffusion of Ge on Si(111). Results are from simulation except as noted.

	Raw activation energy (eV)	Scaled activation energy (eV)[a]	Prefactor (cm^2/s)
Intrinsic exchange	1.9± 0.3	1.3± 0.2	$8\times10^{-2\pm1}$
Intrinsic site hopping	0.87± 0.13	0.59± 0.09	$2\times10^{-3\pm0.5}$
Adatom coverage	2.4± 0.3	1.6± 0.2	$3\times10^{4\pm1}$ [c]
Mass transfer (from $D_{\rm hop}$, θ)	3.3± 0.3	2.2± 0.2	$6\times10^{1\pm1}$
Mass transfer (direct from sim)	3.6± 0.3	2.4± 0.2	$2\times10^{2\pm1}$
Mass transfer (SHM expt)	2.48± 0.09	2.48± 0.09[b]	$6\times10^{2\pm0.5}$

[a]Raw energy multiplied by $T_{m,e}/T_{m,s}=1683$ K/2500 K.
[b]Experimental energy not rescaled.
[c]No units.

To make direct comparisons between our simulations with the stiffened lattice and real experiments, we have drawn on an experimental correlation discovered in the early 1970s for fcc metals.[33] Mass-transfer diffusion results yielded a single universal curve in Arrhenius form when plotted as a function of T_m/T as opposed to $1/T$. From this observation came a simple linear relation between $E_{\rm diff}$ for mass-transfer diffusion and T_m. Preexponential factors, computed in the limit $T\rightarrow\infty$, required no rescaling for direct comparison.

This correlation for $E_{\rm diff}$ suggests that the simulational activation energies should be rescaled by the factor $T_{m,e}/T_{m,s}$ for direct comparison to experiment. Table I shows both raw and rescaled results for $E_{{\rm diff},M}$, $E_{{\rm diff},I}$, and ΔH_f. The second column of numbers in Table I lists the rescaled activation energies from the simulation; the scaling factor lies very near $\frac{2}{3}$. In making this presentation, we have generalized the correlation for fcc metals to include semiconductors. Furthermore, we have assumed that the rescaling for the composite parameter $E_{{\rm diff},M}$ applies to each of its components $E_{{\rm diff},I}$ and ΔH_f. Underlying these assumptions is the notion that T_m, $E_{{\rm diff},I}$, and ΔH_f all depend on the strength with which the substrate can form chemical bonds. A decrease in bonding affinity should decrease all these quantities to roughly the same extent.

Within this framework, intrinsic diffusion by site hopping and by exchange receive the same scaling factor. Since exchange involves the underlying lattice more intimately than site hopping, artificial lattice stiffening might influence exchange somewhat more. We cannot resolve this issue at present. However, the activation energies of the two mechanisms are spread sufficiently to make unlikely a change in our qualitative conclusion about their relative importance under experimental conditions.

For intrinsic site hopping, no experimental data exist to our knowledge for Ge/Si(111). A report does exist for Ge/Si(100), however;[45] island growth studies by transmission electron microscopy and Rutherford backscattering have yielded $E_I=0.83\pm0.13$ eV. Although this number agrees better with our raw (0.87 eV) rather than rescaled (0.59 eV) activation energy from simulation, we point out that many experimental measurements of E_I on Si(111) fall much below their (100) counterparts. Examples include Ag [0.39 eV for (111) vs 0.69 eV for (100) (Ref. 46)], Sn [0.32 eV vs 1.0 eV (Refs. 47 and 48)], and Ga [0.48 eV vs 0.76 eV (Refs. 47 and 48)]. The prefactor we determined falls closely in line with experimental averages for semiconductors near 10^{-3} cm^2/s.[3]

For intrinsic exchange, no experimental data exist to our knowledge for semiconductors. All data currently involve metals, although apparently only one case exists where monomer site hopping and exchange may be compared directly: Ir/Ir(110).[49] In this case, $E_{\rm diff}$ for exchange (0.71 eV) fell slightly below that for site hopping (0.80 eV) while D_0 fell an order of magnitude lower, although in light of experimental uncertainty the difference was not considered significant. These trends run counter to our simulation. However, MD simulations of exchange on Cu(100) do match our trend.[27] $E_{\rm diff}$ for exchange (0.85 eV) fell a factor of 2 above that for hopping (0.44 eV), in line with our results. D_0 for exchange exceeded that for site hopping by slightly over an order of magnitude, compared to our factor of 60. However, it is well known that the precise details of the potential employed can affect such comparisons dramatically.[50]

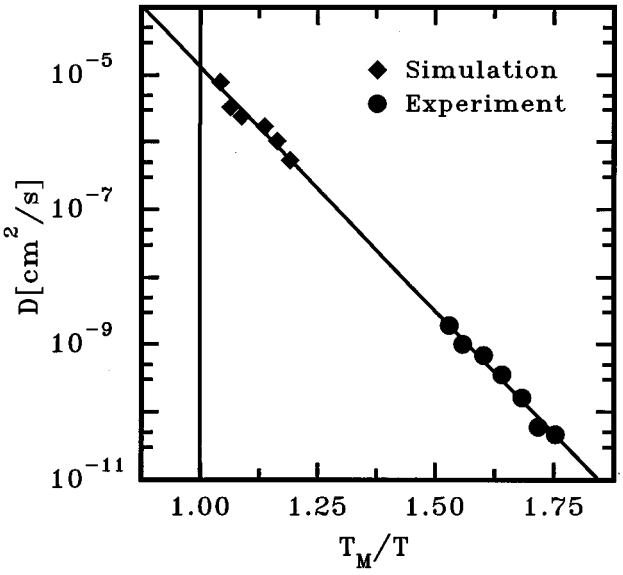

FIG. 10. Direct comparison of mass-transfer diffusivities obtained by simulation and SHM. $T_m=2500$ K for simulation and 1683 K for SHM. Line represents least-squares fit through the simulation data.

For mass-transfer diffusion, direct comparison of simulation with experiment appears in Fig. 10. The abscissa shows reciprocal temperature cast as T_m/T, which constitutes another way of rescaling the simulational data. The line represents the least-squares fit through the simulational data, and runs through the experimental data essentially perfectly. The agreement is particularly striking because the temperature range differs significantly for the two data sets, resulting in the need to extrapolate D over four to five orders of magnitude. Table I shows the agreement in a different form; $E_{\rm diff}$ for the two data sets differs by only 0.1 eV, while D_0 differs by about a factor of 3. The differences in $E_{\rm diff}$ and D_0 compensate each other, however, leading to the good pictorial correspondence in Fig. 10.

While it is true that this close agreement required scaling the simulational data to remove effects of artificial lattice stiffening, the results still inspire substantial confidence in the ability of the Stillinger-Weber potential to model surface diffusion accurately on group-IV substrates. Since many of the atomic-scale islanding phenomena observed in simulation took place on a 10–50-ps time scale, far beyond the reach of current experimental methods, simulations appear to provide the only way to examine such phenomena for the present.

The present work may offer an unusual case of diffusive motion in strongly interacting systems; considerable simplicity characterizes the quantitative description. As remarked earlier, atomic clusters formed easily in the simulations, but monomers, dimers, and trimers exhibited comparable mobilities. This similarity may account for our ability to successfully extrapolate the simulational data into the experimental range. Furthermore, the similarity may account for the lack of coverage dependence in the experimentally derived diffu-

sivities. One would normally expect a coverage dependence to arise in systems with substantial clustering. The reason why quantitative simplicity emerges from the physical complexity of this adsorption system remains a mystery to us.

Of course, the Ge/Si system provided a particularly favorable case for a potential like the Stillinger-Weber. Similar electronegativity and bonding characteristics of the two species made the parameters for the potential easy to quantify and minimized change transfer effects that can affect diffusion substantially.[12] The latter phenomena show up clearly even for diffusion of group-III and -V elements on Si and Ge,[12] and appear to become much larger for alkali metals and other easily ionized species.[3] Nevertheless, the present work provides confidence that many other important features of surface diffusion may be modeled accurately by MD.

D. Comparison with thermodynamic estimates

We have recently presented a fairly detailed set of semiempirical guidelines for estimating diffusional activation energies and prefactors on a wide variety of metals, semiconductors, and insulators.[3] The correlations treat both intrinsic and mass-transfer diffusion, and employ as their basis easy-to-find numbers like desorption energies and bulk-vacancy formation energies. In this section we compare for Ge/Si the results of this algorithm with experiment and simulation.

For intrinsic diffusion on semiconductors, the correlations implicitly address only site hopping, since exchange has not been observed experimentally. The operative equation is

$$E_I = 0.6E_{\mathrm{des}}/M, \tag{10}$$

where E_{des} represents the desorption energy and M denotes the number of bonds the adsorbed atom makes with the substrate. Here we take $M=3$. To our knowledge E_{des} remains unmeasured for Ge and Si, but an average of sublimation energies should provide a satisfactory substitute. These energies are 3.5 and 3.7 eV for Ge and Si, respectively,[51] leading to $E_{\mathrm{des}}=3.6$ eV. Equation (10) then yields $E_I=0.72$, reasonably close to the 0.59 eV obtained from simulation.

For mass-transfer diffusion we must employ Eqs. (3) and (4), preferably with experimental values for E_I and $D_{0,I}$ if possible. However, ΔH_f and ΔS_f almost always require estimation. For semiconductors, ΔH_f equals $\frac{2}{3}$ of the bulk value for the substrate in this framework. With a bulk vacancy energy for Si of 2.5 eV,[52,53] ΔH_f becomes 1.7 eV. This number falls very close to the scaled formation energy of 1.6 eV observed in simulation. The expected lack of ionization effects for Si-Ge makes further correction[3] unnecessary. Entropic effects are more difficult to estimate, even in the absence of ionization. Contributions arise both from lattice softening near a vacancy and from site occupation statistics. The correlation lumps these effects together into $\Delta S_f/k_B$ of roughly 16, leading to a prefactor for vacancy formation of 8×10^6. This value falls significantly above that of 2.7×10^4 drawn from simulation.

Putting these estimates together yields $E_M=2.4$ eV and $D_0=8\times10^3$ cm^2/s for mass transfer. The activation energy lies within 0.1 eV of both the simulational and the experimental results. The prefactor lies one order of magnitude above the experimental value—as good as one can expect for correlations of this type, where, for example, no provision is made for effects of crystallographic orientation.

V. CONCLUSION

This work presents experimental surface diffusion parameters for Ge/Si (111) at high temperature, and shows that molecular-dynamics simulations with a Stillinger-Weber potential can reproduce these numbers quite well. A previously developed semiempirical correlation also does fairly well. However, this work also confirms previous observations that group-IV semiconductors require large ensemble sizes in order to avoid substantial artificial lattice stiffening. This extra effort should prove rewarding, as high-temperature diffusion phenomena appear to involve substantial islanding and clustering effects on picosecond time scales—far beyond the capabilities of current experimental methods. More general application of MD simulation to diffusion of elements with disparate electronegativities will require new potentials that can account for change transfer effects, at least crudely.

ACKNOWLEDGMENTS

This work was supported in part by the National Science Foundation under Grant No. CTS 95-06519. C.E.A. and R.D. acknowledge support from the Department of Energy through the Materials Research Laboratory at the University of Illinois under Contract No. DEFG02-91ER45439.

*Author to whom correspondence should be addressed.

[1] G. Somorjai, *Principles of Surface Chemistry* (Prentice-Hall, Englewood Cliffs, NJ, 1972), p. 101.
[2] C. E. Allen and E. G. Seebauer, J. Chem. Phys. **104**, 2557 (1996).
[3] E. G. Seebauer and C. E. Allen, Prog. Surf. Sci. **49**, 265 (1995).
[4] R. Gomer, Rep. Prog. Phys. **53**, 917 (1990).
[5] V. Hoffman, J. Griswold, D. Mintz, and D. Harra, Thin Solid Films **153**, 369 (1987).
[6] R. Gomer, in *Surface Mobilies on Solid Materials*, edited by V. T. Binh (Plenum, New York, 1981), p. 1.
[7] H. P. Bonzel, in *Structure and Properties of Metal Surfaces*, edited by S. Shimodiara (Maruzen, Tokyo, 1973), Vol. 1, p. 248.
[8] C. Zener, J. Appl. Phys. **22**, 372 (1951).
[9] K. A. Schultz and E. G. Seebauer, J. Chem. Phys. **97**, 6958 (1992), and references therein.
[10] I. I. Suni and E. G. Seebauer, Surf. Sci. **301**, L235 (1994).
[11] I. I. Suni and E. G. Seebauer, Thin Solid Films **272**, 229 (1996).
[12] C. E. Allen, R. Ditchfield, and E. G. Seebauer, J. Vac. Sci. Technol. A **14**, 22 (1996).
[13] C. E. Allen and E. G. Seebauer, Langmuir **11**, 186 (1995).
[14] I. I. Suni and E. G. Seebauer, J. Chem. Phys. **100**, 6772 (1994).
[15] Y. Wang, M. J. Bronikowski, and R. J. Hamers, J. Phys. Chem. **98**, 5966 (1994).
[16] Y. Wang and R. J. Hamers, Phys. Rev. Lett. **74**, 83 (1995).
[17] Y. Wang, X. Chen, and R. J. Hamers, Phys. Rev. B **50**, 4534 (1994).
[18] K. A. Schultz and E. G. Seebauer, J. Opt. Soc. Am. B **10**, 546 (1993).
[19] K. A. Schultz and E. G. Seebauer, Rev. Sci. Instrum. **63**, 218 (1992).

[20] K. A. Schultz, I. I. Suni, C. E. Allen, and E. G. Seebauer, Surf. Sci. **276**, 40 (1992).
[21] R. W. J. Hollering, A. J. Hoeven, and J. M. Lenssinck, J. Vac. Sci. Technol. A **8**, 3194 (1990).
[22] F. H. Stillinger and T. A. Weber, Phys. Rev. B **31**, 5262 (1985).
[23] K. Ding and H. C. Anderson, Phys. Rev. B **34**, 6987 (1986).
[24] M. Laradji, D. P. Landau, and B. Dunweg, Phys. Rev. B **51**, 4894 (1995).
[25] G. L. Kellogg, Surf. Sci. Rep. **21**, 1 (1994).
[26] A. G. Naumovets and Yu. S. Vedula, Surf. Sci. Rep. **4**, 365 (1985).
[27] G. A. Evangelakis and N. I. Papanicolaou, Surf. Sci. **347**, 376 (1996).
[28] G. L. Kellogg, T. T. Tsong, and P. Cowan, Surf. Sci. **70**, 485 (1978).
[29] R. M. Noyes, Prog. React. Kinet. **1**, 129 (1961).
[30] M. P. Seah, *Practical Surface Analysis by Auger X-ray Photoelectron Spectroscopy* (Wiley, New York, 1983) Chap. 5.
[31] S. Ichimura and R. Shimizu, Surf. Sci. **112**, 386 (1981).
[32] M. P. Seah and W. A. Dench, Surf. Interface Anal. **1**, 1 (1979).
[33] H. P. Bonzel, *Structure and Properties of Metal Surfaces* (Maruzen, Tokyo, 1973).
[34] X. J. Chen, F. Ercolessi, A. C. Levi, and E. Tosatti, Surf. Sci. **264**, 207 (1992).
[35] B. Z. Olshanetski, S. M. Repinsky, and A. A. Shklyaev, Pis'ma Zh. Eksp. Teor. Fiz. **27**, 403 (1978) [JETP. Lett. **27**, 378 (1978)].
[36] K. Fukutani, Surf. Sci. **281**, 284 (1991).
[37] E. Ganz, S. K. Theiss, I.-S. Hwang, and J. Golovchenko, Phys. Rev. Lett. **68**, 1567 (1992).
[38] H. Hibino and T. Ogino, Surf. Sci. **328**, L547 (1995).
[39] C. Roland and G. H. Gilmer, Phys. Rev. B **46**, 13 428 (1992).
[40] D. Srivastava and B. J. Garrison, Phys. Rev. B **46**, 1472 (1992).
[41] C. Roland and G. H. Gilmer, Phys. Rev. B **47**, 16 286 (1993).
[42] A. P. Horsfield and P. Clancy, Mater. Sci. Eng. **2**, 277 (1994).
[43] F. F. Abraham and J. Q. Broughton, Phys. Rev. Lett. **56**, 734 (1986).
[44] U. Landman, W. D. Luedtke, R. N. Barnett, C. L. Cleveland, M. W. Ribarsky, E. Arnold, S. Ramesh, H. Baumgart, A. Martinez, and B. Khan, Phys. Rev. Lett. **56**, 155 (1986).
[45] M. Zinke-Allmang and S. Stoyanov, J. Appl. Phys. **29**, L1884 (1990).
[46] M. Hanbucken, M. Futamoto, and J. A. Venables, Surf. Sci. **147**, 433 (1984).
[47] M. Zinke-Allmang and L. E. Feldman, Surf. Sci. **191**, L749 (1987).
[48] M. Zinke-Allmang, L. C. Fedlman, and S. Nakahara, Appl. Phys. Lett. **51**, 975 (1987).
[49] T. T. Tsong and C. C. Chen, Surf. Sci. **246**, 13 (1991).
[50] K. D. Shiang, C. M. Wei, and T. T. Tsong, Surf. Sci. **301**, 136 (1994).
[51] Calculated from data in *CRC Handbook of Chemistry and Physics*, 60th ed, edited by R. C. Weast (CRC, Boca Raton, FL, 1979).
[52] J. A. Van Vechten, Phys. Rev. B **11**, 3910 (1975).
[53] D. Maroudas and R. A. Brown, Phys. Rev. B **47**, 1562 (1993).